

This article was downloaded by:

On: 21 January 2011

Access details: *Access Details: Free Access*

Publisher *Taylor & Francis*

Informa Ltd Registered in England and Wales Registered Number: 1072954 Registered office: Mortimer House, 37-41 Mortimer Street, London W1T 3JH, UK



International Journal of Polymer Analysis and Characterization

Publication details, including instructions for authors and subscription information:

<http://www.informaworld.com/smpp/title~content=t713646643>

Thin Films and Interfaces at High Pressure

Thomas Jakob^a; Gerd Kleideiter^a; Wolfgang Knoll^a

^a Max-Planck-Institut für Polymerforschung, Mainz, Germany

Online publication date: 16 August 2010

To cite this Article Jakob, Thomas , Kleideiter, Gerd and Knoll, Wolfgang(2004) 'Thin Films and Interfaces at High Pressure', *International Journal of Polymer Analysis and Characterization*, 9: 1, 153 – 175

To link to this Article: DOI: 10.1080/10236660490890538

URL: <http://dx.doi.org/10.1080/10236660490890538>

PLEASE SCROLL DOWN FOR ARTICLE

Full terms and conditions of use: <http://www.informaworld.com/terms-and-conditions-of-access.pdf>

This article may be used for research, teaching and private study purposes. Any substantial or systematic reproduction, re-distribution, re-selling, loan or sub-licensing, systematic supply or distribution in any form to anyone is expressly forbidden.

The publisher does not give any warranty express or implied or make any representation that the contents will be complete or accurate or up to date. The accuracy of any instructions, formulae and drug doses should be independently verified with primary sources. The publisher shall not be liable for any loss, actions, claims, proceedings, demand or costs or damages whatsoever or howsoever caused arising directly or indirectly in connection with or arising out of the use of this material.

Thin Films and Interfaces at High Pressure

**Thomas Jakob, Gerd Kleideiter, and
Wolfgang Knoll**

Max-Planck-Institut für Polymerforschung, Mainz,
Germany

This contribution summarizes the design and implementation of a novel experimental tool for the investigation of thin polymer films and interfacial architectures: a classical surface plasmon spectrometer is combined with a high pressure cell, thus allowing for the optical characterization of polymer layers at pressures up to 200 MPa and over a temperature range of 10° to 120°C.

We demonstrate the excellent performance of this combination setup by presenting a few typical results obtained with this instrument. These include, first, the determination of the pressure- and temperature-dependent refractive indices of the pressurizing media used in these studies, i.e., water, methanol, ethanol, and supercritical CO₂ (scCO₂), the pressure dependence of the glass transition temperature in thin poly(ethylmethacrylate) films, and the pressure-dependent collapse behavior of surface-grafted poly(N-isopropylacrylamide) gels in water.

The final example then concerns a further extension of the setup by an electrochemical cell offering investigation of processes like heterogeneous electron transfer reactions at high pressure. We demonstrate by a few results obtained with the electropolymerization of bithiophene that the pressure is not only a thermodynamic variable that determines – just like the temperature – the physical properties of thin films, but it also constitutes an important process parameter during the preparation of polymer coatings.

This summary is based on results obtained in collaboration with a number of colleagues. Thanks are due, in particular, to Prof. M. Lechner, Osnabrück, M. Harmon and Prof. C. Frank, Stanford University, and U. Fehrenbacher and Prof. M. Ballaut, Karlsruhe. Part of this material is based upon work supported by the Science and Research Council, Singapore under Grant Number MCE/TP/00/001.2.

Address correspondence to Wolfgang Knoll, Max-Planck-Institut Für Polymerforschung, Ackermannweg 10, 55128 Mainz, Germany. E-mail: knoll@mpip-mainz.mpg.de

Keywords:

INTRODUCTION

Evanescent wave optics, e.g., surface-plasmon and optical waveguide spectroscopies, are well-established methods for the characterization of interfaces and thin films^[1]. Typically, such studies are performed at room temperature, but temperature-dependent investigations can also be easily performed^[2]. Examples from our group are the waveguide-spectroscopic characterization of the phase behavior (as it manifests itself in the optical properties) of liquid-crystalline (LC) materials in the thin layer of an LC cell^[3,4], and the analysis of the thermal expansion coefficient and the glass-transition temperature of thin and ultrathin polymer films of different molecular architectures^[5].

For practical applications, the pressure may not be as important a parameter as the temperature, but from a fundamental point of view both are thermodynamic variables that control the phase behavior and hence the property profiles of organic or polymeric systems in a rather complementary way^[6].

Hence, a complete picture of the structure-property relation of interfacial architectures and thin films requires a comprehensive analysis of both the temperature and the pressure dependence of the relevant materials' parameters.

To this end, we designed and constructed a surface-plasmon and waveguide spectrometer combined with a high pressure cell that allows for reflectivity measurements with thin films at pressures up to 200 MPa and over a temperature range of 20°–120°C^[6,7].

In this summary report we describe a few of the studies that we performed with this instrument. We first give a very brief outline of the optical techniques employed for the characterization of optical and structural properties of the various thin film samples and describe the specifics of the combination setup for the high pressure studies. Rather than giving a detailed analysis of each of the systems studied, we just present a few features that demonstrate the kind of information that can be gained with this instrument in an attempt to document the potential of pressure-dependent measurements.

We first describe the behavior of a thin polymer film as one scans the temperature at different pressures in the sample cell, thus gaining information on the pressure dependence of the glass transition temperature^[7].

Next, the counteracting effects of temperature and pressure variations will be demonstrated in studies of the collapse behavior of an aqueous polymer gel with a lower critical solution temperature (LCST). We will

demonstrate that changing the pressure can be used as efficiently as varying the temperature in order to induce the collapse of the gel as well as trigger its re-swelling^[8].

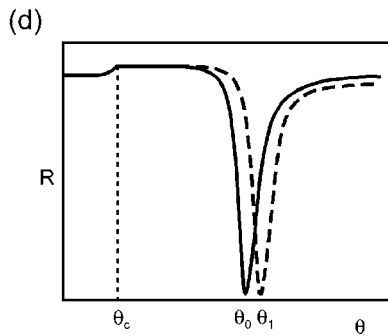
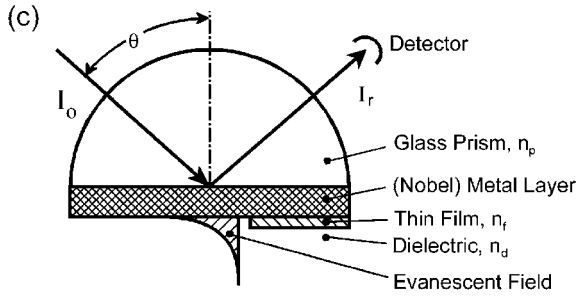
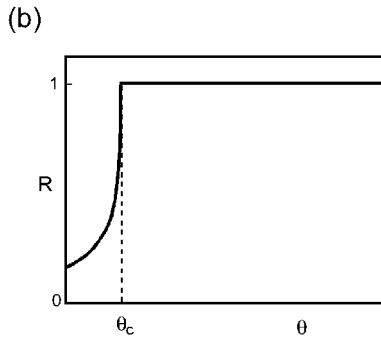
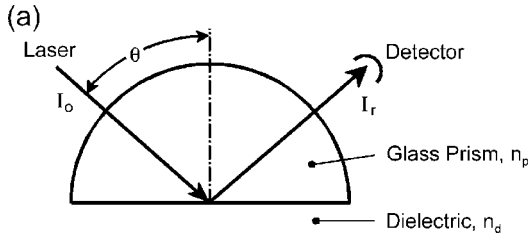
Another interesting series of experiments can be performed with supercritical CO₂ used as the pressure medium. Its low refractive index even in the liquid state makes it a particularly interesting solvent for optical studies with a very high contrast relative to the polymer film^[9]. The final set of experiments described concerns a further extension of the experimental options by coupling an electrochemical setup to the high pressure SPR instrument. We will conclude this review presentation by describing some preliminary studies of the pressure dependence of the synthesis of polymer layers by electropolymerization^[10].

SURFACE-PLASMON AND WAVEGUIDE SPECTROSCOPIES

The basic principles of evanescent optical waves in the special formats of plasmon surface polaritons (or surface plasmons for short) and guided optical modes in slab waveguides have been described in great detail in the literature^[1,11]. We give only a very brief summary introduction here.

Figure 1(a) starts with the well-known total internal reflection geometry: a laser beam of intensity I_0 (in the experiments described below typically from a HeNe laser operated at $\lambda = 633$ nm) incident on a (high refractive index n_p) glass prism is reflected off the base of the prism in contact to a (dielectric) medium of refractive index n_d . As one changes the angle of incidence, θ , the reflected intensity I_r varies strongly: for small angles most of the incident light is transmitted and, hence, the reflectivity $R = I_r/I_0$ is very low. This is shown in Figure 1(b). As one approaches the so-called critical angle, θ_c , the reflectivity increases strongly and reaches unity for $\theta > \theta_c$, i.e., above the critical angle no light is transmitted but the complete intensity is (totally internally) reflected. According to Snell's law, the critical angle is given by the refractive index of the prism and the dielectric, respectively, $\theta_c = \arcsin(n_p/n_d)$.

For the excitation of surface plasmon modes in the so-called Kretschmann configuration a thin metal film ($d_m \sim 50$ nm) of typically Au or Ag is evaporated onto the base of the prism and the same intensity-versus-angle of incidence experiment performed (Figure 1(c)). (One should mention that in practice the metal is evaporated onto a thin glass slide with the identical refractive index n_p , which is then index-matched to the prism.) For small angles the reflectivity is now rather high because the metal film acts as a mirror (see Figure 1(d)). The critical angle is still seen in the reflectivity scan (and is still given by Snell's law), however, at a characteristic resonance angle, θ_o , the reflectivity drops to virtually zero within a very narrow angular range. The complete reflectivity-versus-angle



of incidence curve can be described by a Fresnel simulation (based on Maxwell's theory) of the reflectivity behavior of a multilayer assembly (in our case, the prism with n_p , the (noble) metal layer described by its complex refractive index, $\tilde{n}_m = n_m + ik_m$, and its thickness d_m , and the dielectric medium of refractive index n_d (note: $n_d^2 = \epsilon_d$).

The general interest in surface plasmon optics originates, to a large extent, from the very sensitive dependence of the angular position of the surface plasmon resonance on the optical architecture near the metal/dielectric interface. For example, any thin film deposited onto the metal layer (see Figure 1(c)) changes the dispersion behavior of the surface plasmon mode and, hence, shifts the angular position of the resonance minimum. Typically, the refractive index of such a thin film coating, n_f , is higher than the dielectric environment, resulting in a shift of the resonance to higher angles, e.g., to θ_1 (see Figure 1(d)), but it could be also in the opposite direction^[12].

It should be noted that despite the shift of the surface plasmon the position of the critical angle, θ_c , remains unchanged upon the deposition of a thin film because also in this case only the dielectric medium with n_d is relevant for Snell's law.

However, should n_p vary during the experiment, e.g., as a function of the temperature or of the applied pressure, both the critical angle, θ_c , and the surface plasmon resonance angle will vary in the same way but can be also simulated quantitatively by the Fresnel algorithm. This will be important for the experiments described below in which the pressure medium (a liquid) will change its optical properties, as will the thin film under investigation.




FIGURE 1 (a) Schematic geometry for total internal reflection (TIR) measurements with a cylindrical prism of refractive index n_p in contact with a dielectric of refractive index n_d . The laser with intensity I_o is incident at an angle θ reflected off the base of the prism, and the reflected intensity, I_r , is monitored by a photodiode detector. (b) Reflectivity, i.e., reflected intensity I_r , divided by the incident intensity I_o , monitored as a function of the angle of incidence, θ , in the TIR geometry of (a). θ_c indicated the critical angle for total internal reflection. (c) Attenuated total internal reflection (ATR) geometry for the excitation of (the evanescent field of) a surface plasmon mode in this Kretschmann setup. The nearly free electron gas in the evaporated thin ($d_m = 50$ nm) noble metal layer acts as a resonator driven by the incident laser beam. (d) ATR scan, i.e., reflectivity, R , versus the angle of incidence, θ , measured in the configuration given in (c) before (full curve) and after (broken curve) the deposition of a thin coating film (cf (c)). (e) For thicker coatings additional resonances appear in the reflectivity scan (f) that are guided optical waves giving additional information about the waveguide material.

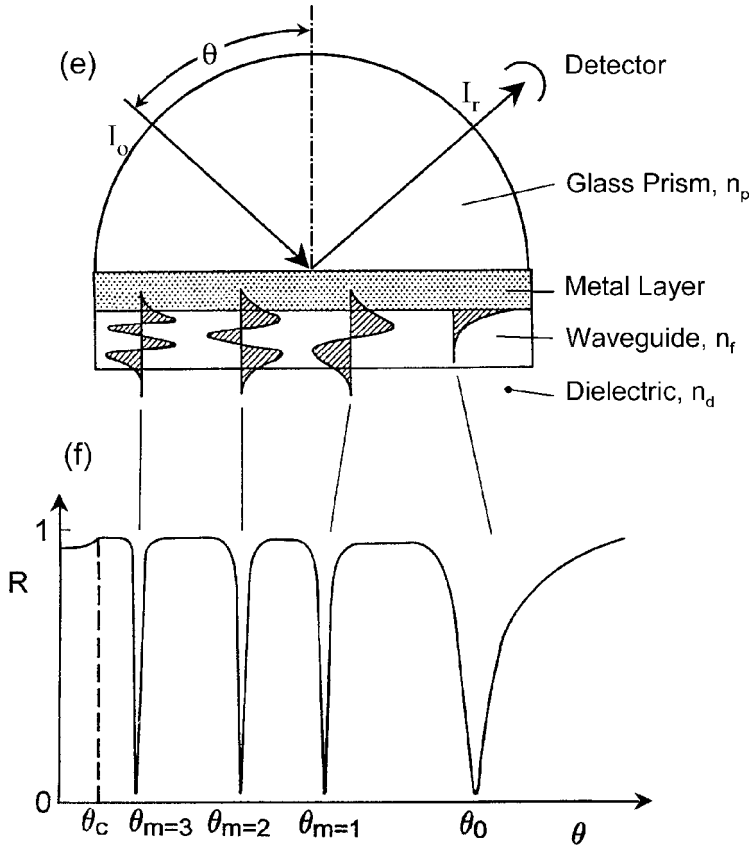


FIGURE 1 (Continued).

For increasing coating thicknesses (with $n_f > n_d$, see Figure 1(e)) the surface plasmon mode keeps shifting to higher resonance angles until above a certain film thickness ($d_f \sim .25 \mu\text{m}$ at $n_f \approx 1.5$ in air, i.e., $n_d = 1.0$) additional resonances can be seen in the reflectivity spectrum (see Figure 1(f)). These are waveguide standing modes with an optical field characteristic similar to Fabry-Perot standing waves (see Figure 1(e)), which propagate, however, within the slab waveguide. The angular positions of the different modes of order m depend for each mode in a unique and characteristic way on the thickness, d_f , and the refractive index, n_f , of the waveguide structure (and, of course, on the refractive index of the bulk dielectric, n_d). The particular analytical advantage of waveguide spectroscopy for the characterization of thin films originates from the fact that these guided modes – other than surface plasmons, which can be

excited only with p-polarized light – can be seen in the reflectivity scans with p- and s-polarized light and, hence, allow for the evaluation of the full indicatrix (i.e., n_{xx} , n_{yy} , n_{zz}) of optically anisotropic media.

Another coupling scheme for surface plasmon excitation used in the following high pressure experiments is based on a grating structure (Figure 2(a)). Typically, a suitable substrate (polymer, glass, Si wafer) with a sinusoidal surface corrugation of periodicity Λ in the range of $\Lambda = 500 \text{ nm} \dots 2 \mu\text{m}$ and an amplitude of a few 10 nm is coated by a (noble) metal layer of $d_m > 150 \text{ nm}$. The resulting grating vector $|\vec{G}| = 2\pi/\Lambda$ allows for a momentum matching scheme illustrated in Figure 2(b) and (c), respectively. At resonance, the (colinear) addition of the photon wavevector projection along the x-direction, k_{ph}^x , and the grating vector \vec{G} match the surface plasmon wavevector, \vec{k}_{sp} , and hence allow for the excitation of the surface plasmon mode.

The energy-momentum dispersion scheme for surface plasmons at metal gratings given in Figure 2(c) illustrates this further. In addition to the two dispersion branches originating from $k_{\text{sp}} = 0$ representing a forward (+x) and backward (-x) propagating surface plasmon mode, further branches start at $\pm n \bullet 2\pi/\Lambda$ (PSP $^{\pm n}$, $n = 1, 2, \dots$). At the given laser energy ω_L , the addition of the photon wavevector projection, k_{ph}^x , and the grating vector \vec{G} allows one to reach a point on the dispersion branches (at +PSP 0 in the example in Figure 2(c)).

Another way of looking at the grating coupling scheme is by realizing that the grating “scatters” the surface plasmon states of a flat surface represented by the dispersion curve PSP 0 from outside the light cone (shaded area in Fig. 2(c) limited by the light line $\omega = \pm c_d k_{\text{ph}}$ with c_d being the speed of light in the dielectric medium above the grating (see Fig. 2(a)) where it cannot be reached by the incident photons into the light cone and, hence, allows for resonant surface plasmon excitation.

EVANESCENT WAVE OPTICS AT HIGH PRESSURE

The high pressure cell that we modified and adapted to perform surface-plasmon and waveguide spectroscopic experiments originally was designed for light scattering and small angle neutron scattering experiments^[13,14]. It uses liquids to pressurize the sample with the advantage that relatively high pressures can be obtained without pumping too much energy into the system because for (nearly) incompressible liquids the term $p\Delta V$ remains small. The main cell body is made of stainless steel with sapphire windows for the optical excitation (Figure 3).

Two types of modifications were realized. In the first one, shown in Figure 3(a), one of the thick sapphire windows is replaced by a thinner one with a high index prism index-matched to it. The inner surface of the sapphire window was coated by a thin metal layer and the sample film thus

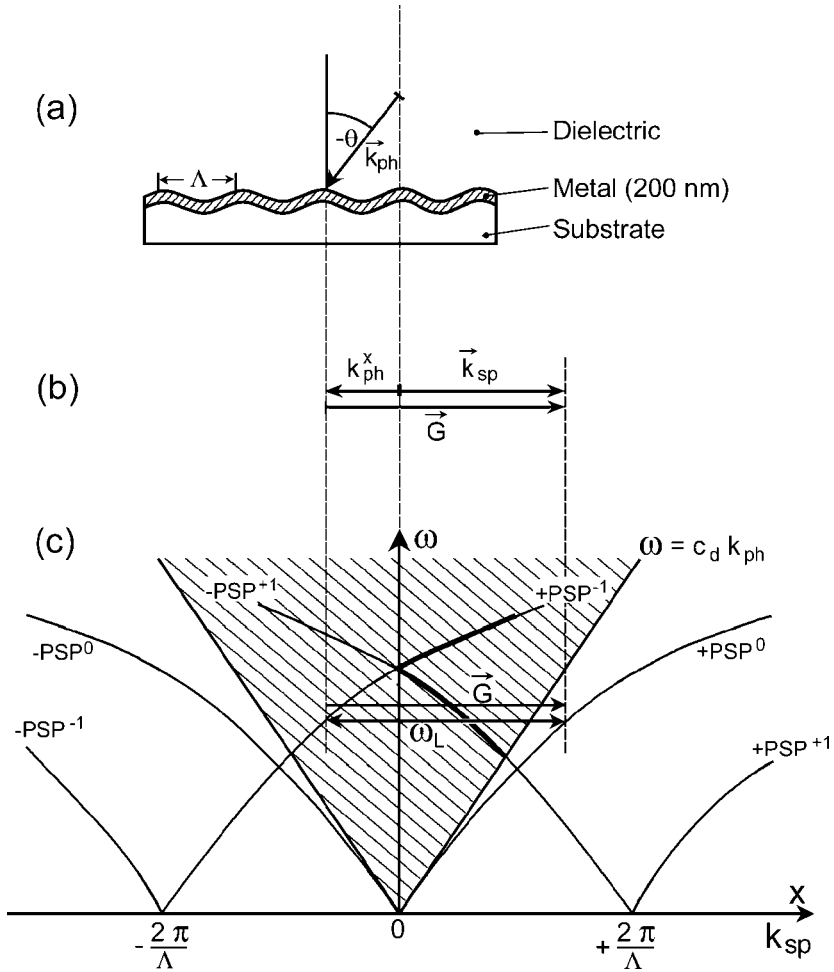


FIGURE 2 (a) Schematic cross section of a grating coupler: a solid substrate with a sinusoidal surface corrugation of periodicity Λ is coated with a (noble) metal layer and in contact with a dielectric. The excitation laser is incident at an angle $-\theta$. (b) Momentum matching scheme between the projection of the incident photon wavevector along the x-axis, k_{ph}^x , the grating vector \vec{G} with $|\vec{G}| = 2\pi/\Lambda$, and the surface plasmon wavevector, k_{sp} . (c) Brillouin zone scheme imposed upon the dispersion of surface plasmon waves by the grating structure, resulting in new dispersion branches that originate – in addition to $k_{sp} = 0$ from $\pm 2\pi/\Lambda$ (noted: $\pm PSP^{\pm n}$). The shaded area between the two light lines ($\omega = \pm c_d k_{ph}$) defines that region of PSP dispersion that can be accessed by the grating coupling scheme.

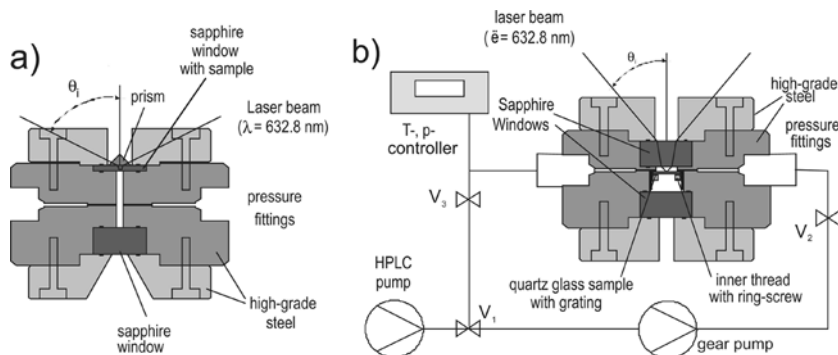


FIGURE 3 Schematic cross section of the high pressure cell for the ATR prism (a) and grating coupling (b) techniques under high pressure up to 1000×10^5 Pa for the former and 2000×10^5 Pa for the latter. For photoisomerization experiments under high pressure, the configuration of the (pump) light irradiation is indicated. For the experiment with scCO_2 , the pressure is built up using an HPLC pump. The gear pump provides for a homogeneous solution in the mixing cycle.

allowing for SPR experiments with the samples being in contact with the pressure medium. Sealing of the two windows was achieved by thin Au wires. A lid in the top steel cover of the cell enabled us to couple the laser via the prism to the surface plasmon resonances at the metal/film/liquid interface.

A major disadvantage of this configuration is the limited pressure range for experiments, i. e., not exceeding approximately 100 MPa, because the thinner sapphire window cannot stand the forces involved at higher pressures.

Thus, an alternative setup based on a grating coupling scheme was designed. The schematics are shown in Figure 3(b). The sample slide with the grating structure and any thin film sample is a separate module placed inside the high pressure cell and is not part of the pressure sealing structure. Thus, both sapphire windows can be thick and robust enough to stand pressures of up to 200 MPa. A slight disadvantage of this setup is the limited angular range available for surface-plasmon or waveguide excitation. However, this can be compensated for by the free choice of the grating periodicity Λ , which allows for tuning of the respective resonance angle to virtually any desired angle of incidence (see also Figure 2(c)).

Also shown in Figure 3(b) is the attachment that is used to operate the setup with supercritical (sc) CO_2 . A high performance liquid chromatograph (HPLC) and additional gear pump are used to fill and pressurize the cell with CO_2 .

Not shown in Figure 3 is the cell jacket that allows for temperature control of the sample volume up to $T = 120^\circ\text{C}$.

OPTICAL PROPERTIES OF THE PRESSURIZING LIQUIDS

As mentioned above the liquids that are used to generate the desired pressure will change their optical constants as a function of pressure (and temperature). This effect has to be quantified before any pressure effects on a thin film sample can be evaluated.

Moreover, one needs to check whether either the prism/window material or the evaporated (noble) metal film do change their optical constants as one applies higher pressure.

In order to test this a series of reference measurements were performed with (a) the sapphire substrate in direct contact with the pressure media (H_2O , methanol, ethanol, scCO_2), i.e., prior to any metal deposition in a total internal reflection (TIR) experiment, and (b) after evaporation of a 50 nm thick Au film.

Some representative data are shown in Figure 4. In addition to TIR scans for the system sapphire/ H_2O at various pressures (as indicated) given in Figure 4(a), a series of SPR angular scans in the Kretschmann setup are given in Figure 4(b).

As mentioned above both the critical angle θ_c , and the surface plasmon resonance angle shift as one increases the pressure. The quantitative evaluation of these experiments confirms that the sapphire and the Au layer do not show any appreciable effect of the pressure (up to 200 MPa) on their optical properties. The refractive indices of the various pressure media, however, show a rather strong dependence of the applied pressure.

This is summarized in Figure 5. The data for H_2O , methanol, and ethanol compare well with literature values and can be fitted by the well-known Lorentz-Lorenz equation, which relates the pressure-dependent mass density of a material with the polarizability described in a Clausius-Mosotti approach. The data of the scCO_2 show the expected low values, with a strong dependence on pressure and temperature. All values would fall onto a straight line as a master curve if plotted as a function of the mass density (not shown).

THIN POLYMER FILMS AT DIFFERENT TEMPERATURES AND PRESSURES

The first series of high-pressure experiments that we present were performed with various thin polymer films. The structure formulas of the employed macromolecules are given in Figure 6.

An example of the pressure dependence of the waveguide mode spectrum measured at room temperature for a poly(methyl methacrylate) (PMMA) film spin-coated onto a Au substrate is shown in Figure 7. The various modes shift to higher resonance angles as one increases

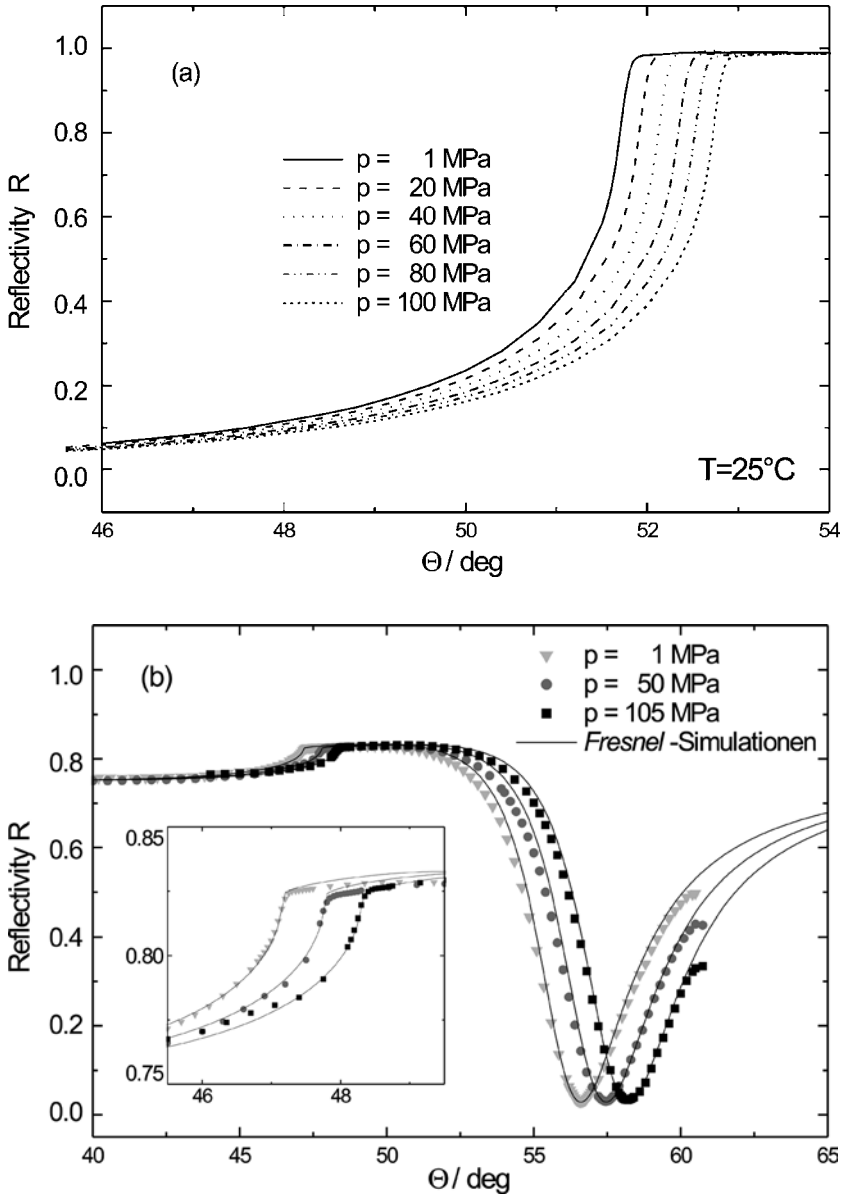


FIGURE 4 (a) TIR scans near the critical angle for total internal reflection θ_c (see Figure 1(b)), taken for the system sapphire/water at various pressures as indicated. (b) ATR scans taken for the system Au/water at different pressures. The symbols are the experimental data points, the full curves are Fresnel simulations that take into account the pressure-dependent refractive index of the liquid, thus describing the angular shift of θ_c and of θ_1 equally well.

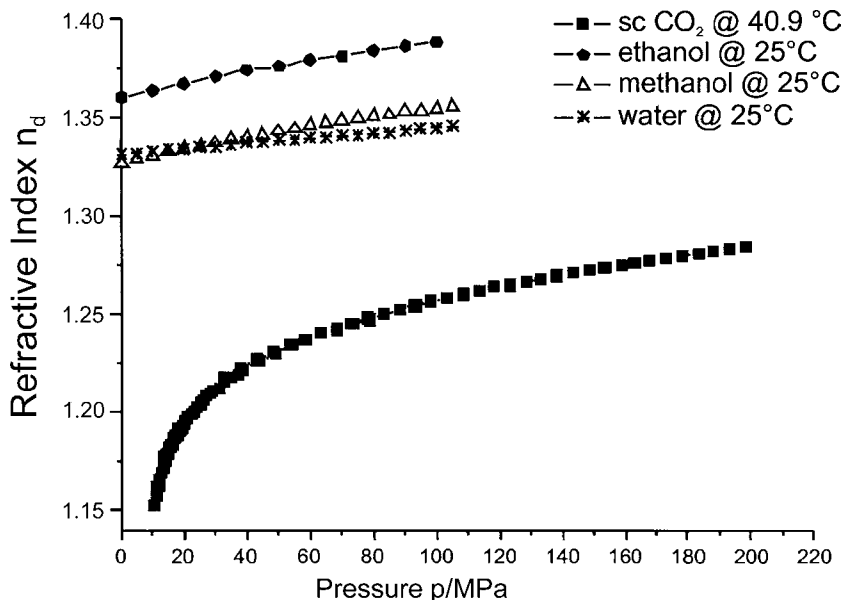


FIGURE 5 Refractive index values, n_d , for water, methanol, ethanol, and supercritical CO₂ (scCO₂) determined as a function of the applied pressure and at the temperatures indicated.

the pressure. The quantitative evaluation has to take into account the pressure dependence of the liquid medium (in this case, H₂O) determined in the reference experiments described above.

The resulting change of the refractive index and the thickness of the thin PMMA film is given in Figure 8. As intuitively expected, the thickness decreases slightly as one increases the pressure in the adjacent aqueous medium, whereas the corresponding densification of the polymer results in a weak increase of the refractive index.

The very opposite behavior is found for a PMMA film of similar thickness pressurized in scCO₂ up to 50 MPa: the thickness increases, whereas the refractive index decreases. The reason for this apparently unusual behavior is the strongly increasing solubility of scCO₂ in PMMA with increasing pressure. The observed thickness increase is a swelling effect by the uptake of solvent into the polymer matrix, with a concomitant decrease of the resulting effective refractive index of the composite.

The next set of experiments concerns the combination of temperature- and pressure-dependent studies aimed at elucidating the pressure-dependent glass transition temperature of poly(ethyl methacrylate) (PEMA).

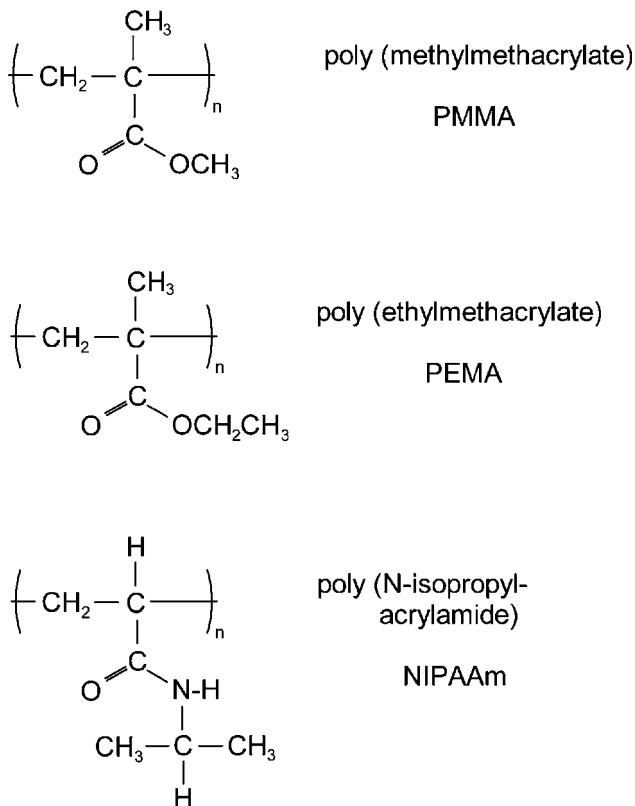


FIGURE 6 Structure formulas of poly(methyl methacrylate) (PMMA), poly(ethyl methacrylate) (PEMA), poly(N-isopropylacrylamide) (NIPAAm).

To this end, SPR scans were taken with a thin polymer film of PEMA, prepared by spin-coating onto a Au-coated substrate, at different pressure values in the cell, while stepwise increasing the temperature. Given in Figure 9(a) are the obtained SPR resonance angles, θ_1 , which reflect the behavior of the optical thickness of the film at the particular temperature and pressure, but also include the optical properties of the pressure medium, H_2O in this case. Relevant for the data analysis is only the fact that the measured values can be approximated for low and high temperatures, respectively, by two straight lines, the intersection of which is interpreted as the glass transition temperature, T_G , of the polymer (at this pressure) separating a region of low thermal expansion below T_G from the phase of high(er) thermal expansion above T_G . The intersections of the linear fits to the data allow for a rather accurate

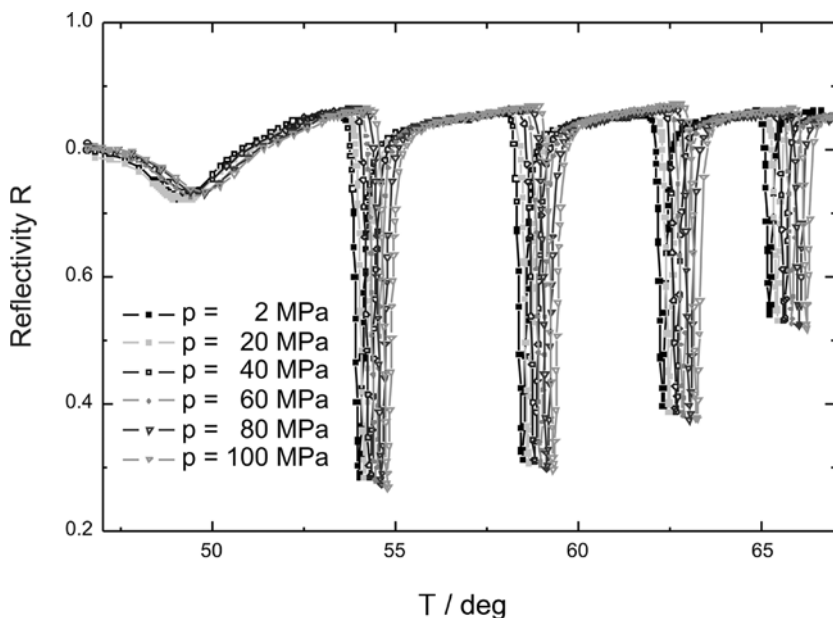


FIGURE 7 Waveguide spectra of a PMMA thin film ($d_f \sim 1.1 \mu\text{m}$) in contact with water, recorded at different pressures, as indicated.

determination of T_G as a function of the applied pressure. The obtained dependence given in Figure 9(b) results in an increase of the glass transition temperature of PEMA of approximately $\Delta T_G = 2^\circ\text{C}$ per 10 MPa pressure increase.

The next set of experiments, i.e., the temperature and pressure dependence of the collapse and swelling behavior of an aqueous NIPAAm gel grafted to a Au-substrate, needs some introduction. In the highly swollen state the gel was much thicker than the extent of the evanescent tail of the surface plasmon mode, which is exponentially decaying and reaches out some 150 nm only. In this situation the surface plasmon “senses” only a highly dilute polymer network in water with a correspondingly low refractive index (close to pure water). This is schematically depicted in Figure 10 (upper illustration). At a temperature commonly referred to as “lower critical solution temperature” (LCST) in the literature the gel collapses and forms a dense film on the substrate, now being much thinner than the extent of the evanescent tail (see Figure 10, lower illustration). As a result, the surface plasmon resonance shifts to higher angles because effectively more of the (collapsed) polymeric material with its higher refractive index is “seen” by the surface mode.

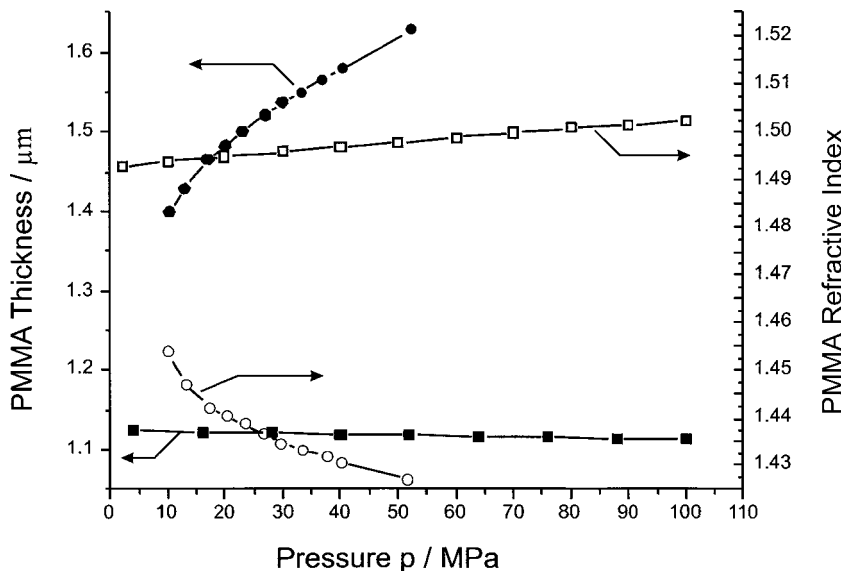


FIGURE 8 Thickness (full symbols) and refractive index (open symbols) of two different PMMA films, one in contact to water (squares), the other in contact to $s\text{CO}_2$ (circles), determined as a function of the pressure in the cell.

The corresponding behavior monitored in the temperature-dependent angular scans performed at normal pressure with a gel prepared on a grating coupler is documented in Figure 11(a). For a series of scans at temperatures below LCST only slight variations of the SPR resonance conditions reflect minor structural changes. However, an abrupt shift between $T = 34^\circ\text{C}$ and $T = 39^\circ\text{C}$ indicates the collapse of the gel.

Analyzing the angular scans results in an effective index of the gel/water system and its temperature dependence. The resulting curves measured for various pressures up to 100 MPa are given in Figure 11(b). Two observations are noteworthy: (i) the cooperativity of the transition is most pronounced at ambient pressure and decreases strongly as one increases the pressure and (ii) the midpoint of the transition (the collapse temperature) shifts to higher temperatures as one increases the pressure.

As a consequence, one can identify temperatures, both in the collapsed and in the swollen state, for which the application of pressure results only in an increase of the overall density and, hence, an increase of the effective refractive index. This is demonstrated in Figure 11(c) for $T = 19.8^\circ\text{C}$ and $T = 57.3^\circ\text{C}$, which is in the fully swollen and in the collapsed state of the gel, respectively.

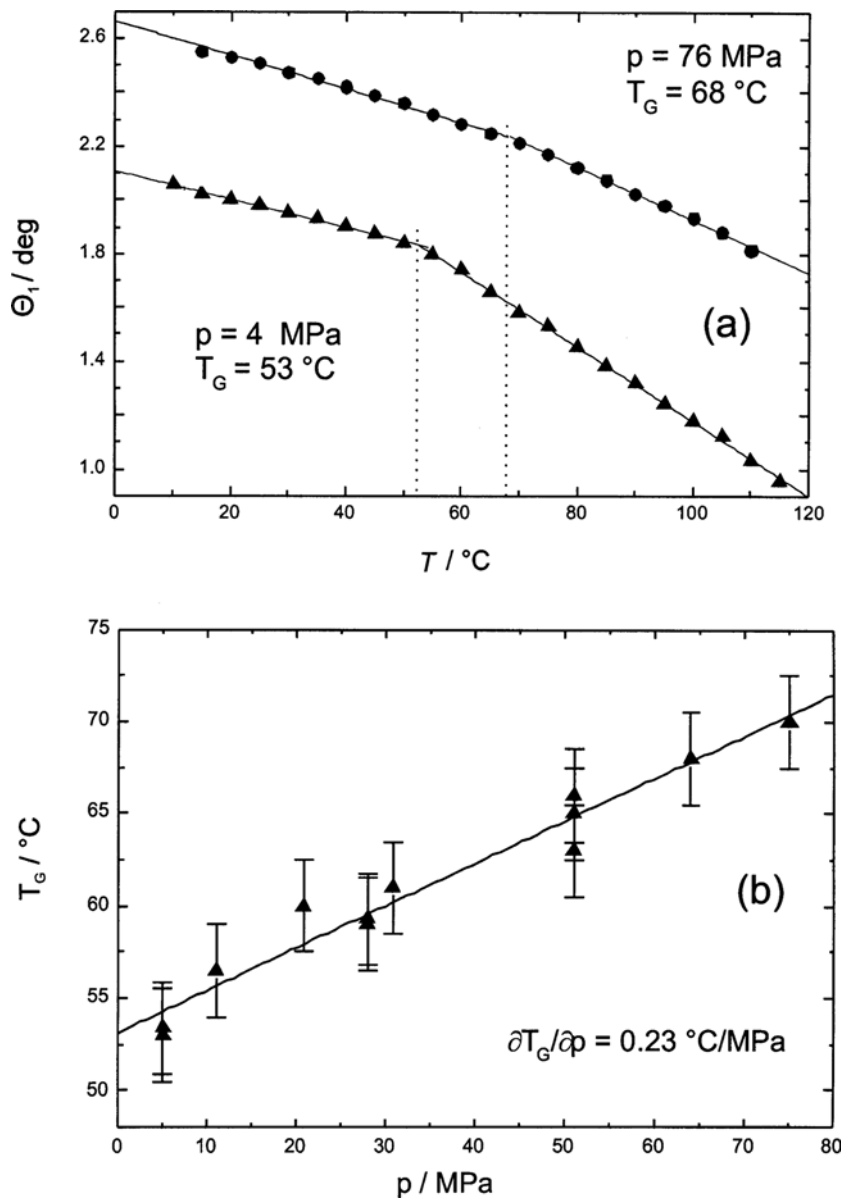


FIGURE 9 (a) Temperature scans of the surface plasmon resonance angle, θ_1 , of a thin PEMA film in contact with water, measured at two different pressures, $p = 4$ MPa and $p = 76$ MPa, respectively. The respective linear fits to the data points intersect at the corresponding glass transition temperature, T_G . (b) Glass transition temperatures, T_G , as determined from plots like the ones given in (a) for various pressures. The linear fit to the data points yields a slope of $2^\circ\text{C}/10$ MPa.

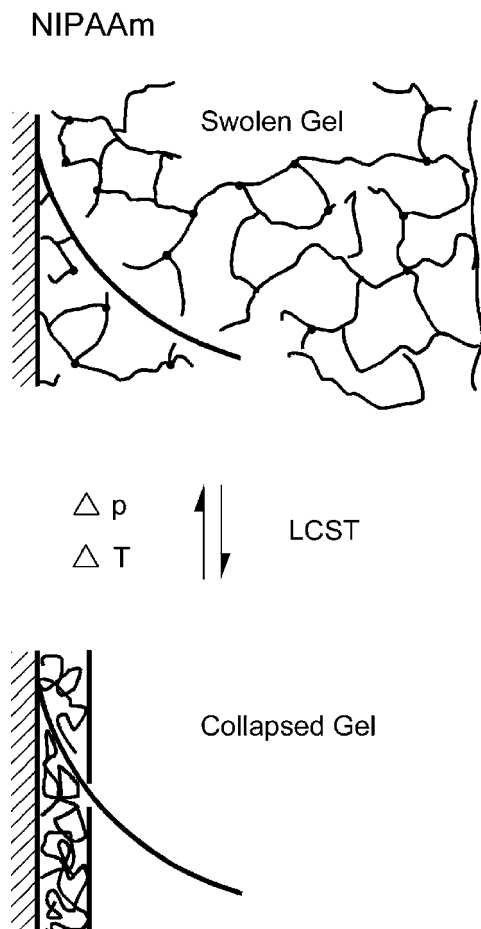


FIGURE 10 Schematic drawing of a swollen NIPAAm gel with a thickness exceeding the evanescent tail of a surface plasmon mode. After the collapse of the gel under the influence of a temperature or pressure change at the lower critical solution temperature (LCST), the compact polymer layer is thinner than the evanescent wave and reaches into the dielectric, resulting in an increase of the effective refractive index n_f of the polymer/water composite.

However, at intermediate temperatures one can find the counteracting effect of increasing the temperature or increasing the pressure. As one can see from Figure 11(b) and as is plotted in Figure 11(c), a collapsed gel at $T = 36.3^\circ\text{C}$ or $T = 39.5^\circ\text{C}$ can be reversibly triggered to re-swelling by increasing the pressure in the cell.

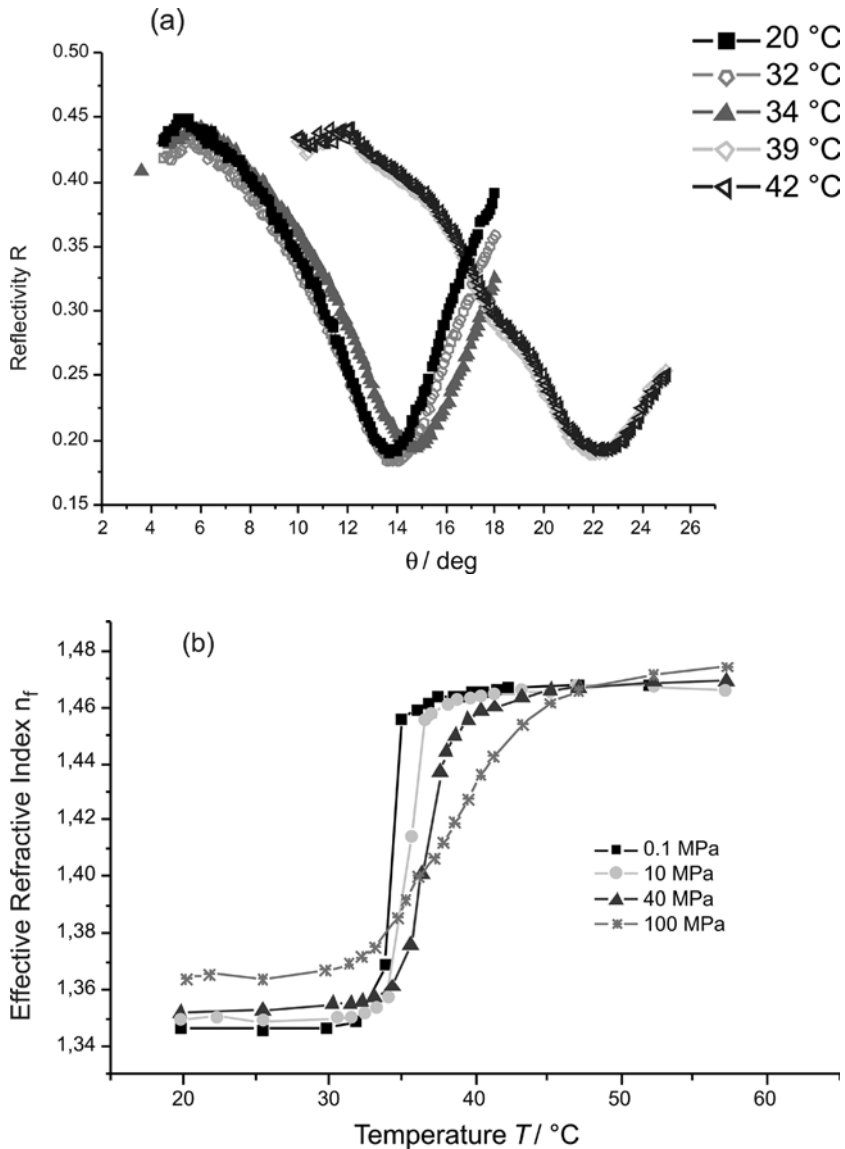


FIGURE 11 (a) ATR reflectivity scans taken at ambient pressure but at different temperatures, as indicated, in the grating coupling scheme of a NIPAAm gel grafted to the grating surface. (b) Effective refractive index values n_r of the NIPAAm/water composite interface, as determined from scans like the ones presented in (a) taken as a function of temperature and at different pressures, as indicated. (c) Effective refractive index values, n_r , obtained as a function of pressure at various temperatures, as indicated.

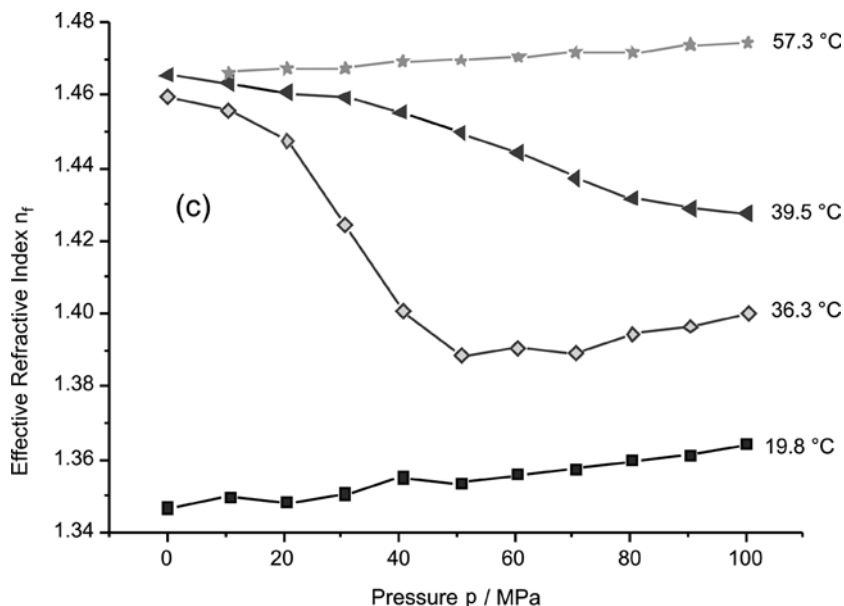


FIGURE 11 (Continued).

ELECTROPOLYMERIZATION AT HIGH PRESSURE

The last set of experiments that we briefly describe concerns a further extension of the experimental setup by an attachment that allows for electrochemical experiments in the high pressure/SPR instrument. A schematic cross section of the modified high pressure cell with the electrode connectors is shown in Figure 12(a). The grating coupler used for surface plasmon excitation was modified by evaporated electrodes so as to contain a central working electrode and a reference electrode (see Figure 12(b)), with the counter electrode being the cell body.

As a first performance test, cyclic voltammetry scans were recorded with $[Fe(CN)_6]^{3-/4-}$ in the electrolyte used as the pressure medium. Figure 13 shows the I-E curves taken at a scan rate of $v = 10$ mV/s at different pressures. The observed response to an increase in pressure – a shift of the formal potential to higher values and a decrease in the peak current – can be fully accounted for by assuming a reduced diffusion coefficient of the redox species to and from the electrode and a slightly increased solvent mass density at higher pressures. From these test studies it was concluded that the special electrode arrangement required to accommodate the pressure cell design allowed for proper electrochemical experiments to be conducted.

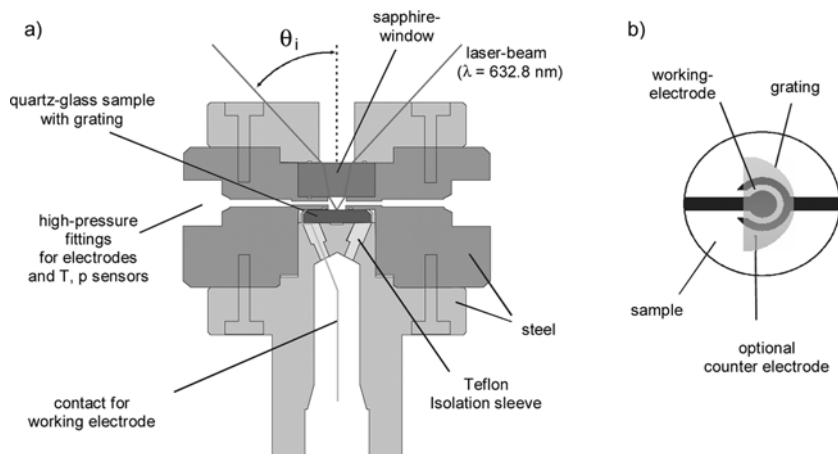


FIGURE 12 (a) Schematic of the cross section of the high pressure cell equipped for electrochemical measurements with grating coupling. (b) Schematic drawing of the glass disk, equipped with a grating and two evaporated electrodes used in the three-electrode electrochemical setup.

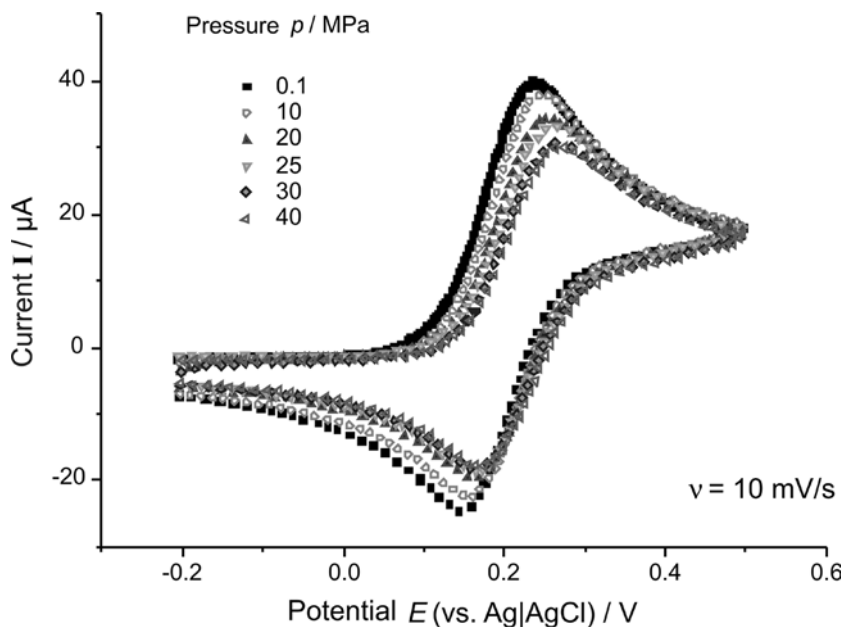


FIGURE 13 Cyclic voltammograms taken at a scan rate of $v = 10 \text{ mV/s}$ between $E = -0.2$ and $E = 0.5 \text{ V}$ (vs. Ag/AgCl) with the electrochemical high pressure cell shown in Figure 12 with $\text{Fe}_2(\text{CN})_6^{3-/4-}$ in the electrolyte.

A first series of electropolymerization studies indicated the strong dependence of the electron-transfer reaction inducing the radical formation and growth of the polymer at the electrode surface on the applied pressure in the cell. Figure 14(a) shows the cyclic voltammograms obtained with 0.05 M bithiophene in the electrolyte solution at moderately increased cell pressures. The redox peaks are significantly shifted upon pressurization of the cell such that for higher values no significant electron transfer occurs anymore within the accessible potential window.

As a consequence, the growth rate of the resulting polymer layer, given in Figure 14(b) as the accumulated thickness versus the number of redox cycles, strongly depends on the applied pressure. The details of this dependence are not fully understood yet but it is obvious that in this case the pressure is not only a variable that controls the physical state of a polymer film but that it is also a major process parameter that may allow

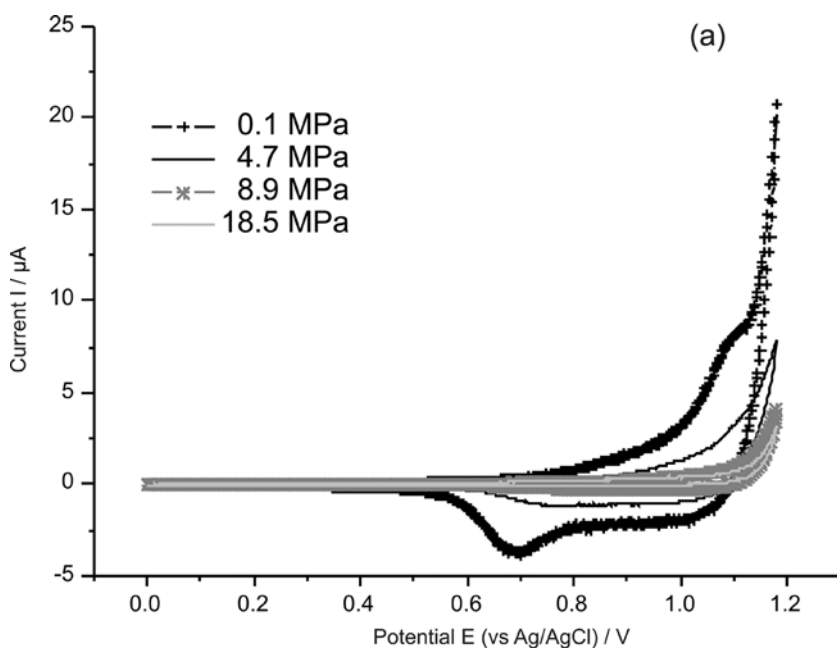


FIGURE 14 (a) Cyclic voltammograms of 0.05 M bithiophene in the electrolyte solution taken at a scan rate of $v = 10 \text{ mV/s}$ between $E = 0.0 \text{ V}$ and $E = 1.15 \text{ V}$ (vs. Ag/AgCl) at different pressures in the electrochemical cell, as indicated. (b) Accumulated thickness data obtained from SPR measurements taken during the electropolymerization (in a cyclic voltammetric mode) of bithiophene at different pressures, as indicated.

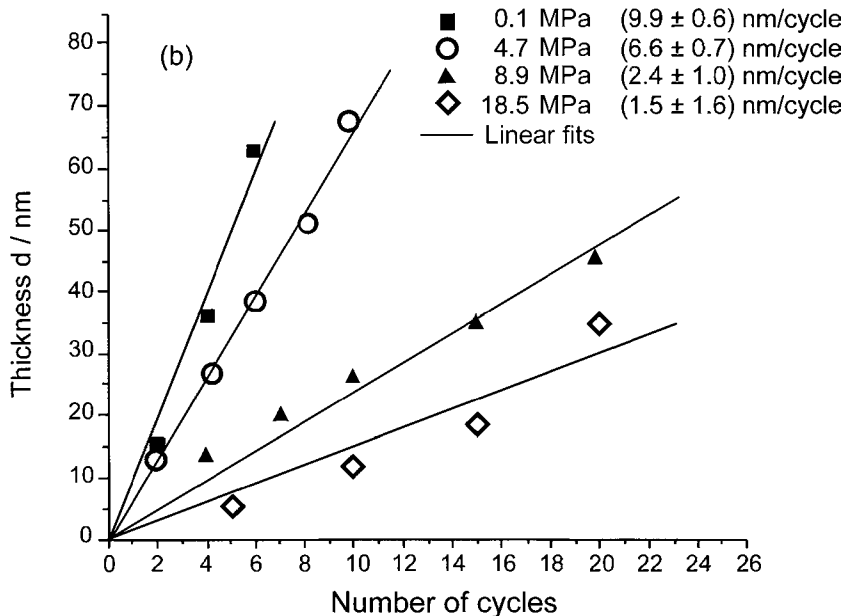


FIGURE 14 (Continued).

for the preparation of films with properties not available with normal electropolymerization conditions.

CONCLUSION

We have demonstrated that the combination of a classical surface plasmon spectrometer – in the Kretschmann prism configuration and/or with grating couplers – with a high pressure cell opens up experimental possibilities to study the physical properties of thin polymer films not only as a function of temperature but also as a function of the applied pressure. This way, a far better understanding of the structure/order – property/function relation of polymeric layers can be gained. The few practical examples that were presented were meant to give only the flavor of what will be possible with this novel combination setup.

The results presented for the electropolymerization of a polythiophene thin film from bithiophene under pressure documented that not only the physical properties of samples prepared at ambient conditions critically depend on the applied pressure during the examination, but the pressure is also an important process parameter that seems to allow for the

preparation of polymer films with structures and properties not accessible by preparation protocols at ambient pressure.

REFERENCES

- [1] Knoll, W. (1998). *Ann. Rev. Phys. Chem.* **49**, 569–638.
- [2] Prucker, O., S. Christian, H. Bock, J. Rütke, C.W. Frank, and W. Knoll. (1998). In *Organic Thin Films*, Washington, D.C.: American Chemical Society; pp. 233–249.
- [3] Ito, S., M. Mitsuishi, M. Yamamoto, T. Fischer, F. Kremer, and W. Knoll. (1993). *Ferroelectrics* **148**, 369–378.
- [4] Ito, S., F. Kremer, E. Aust, and W. Knoll. (1994). *J. Appl. Phys.* **75**, 1962–1967.
- [5] Prucker, O., S. Christian, H. Bock, J. Rütke, C.W. Frank, and W. Knoll. (1998). *Macromol. Chem. Phys.* **199**, 1435–1444.
- [6] Kleideiter, G., M. D. Lechner, and W. Knoll. (1999). *Macromol. Chem. Phys.* **200**, 1028–1033.
- [7] Kleideiter, G., O. Prucker, H. Bock, C.W. Frank, M. D. Lechner, and W. Knoll. (1999). *Macromol. Symp.* **145**, 95–102.
- [8] Harmon, M., T. Jakob, W. Knoll, and C. Frank. (2002). *Macromolecules* **35**, 5999–6004.
- [9] Fehrenbacher, U., T. Jakob, T. Berger, W. Knoll, and M. Ballauff. (2002). *Fluid Phase Equilibria* **200**, 147–169.
- [10] Jakob, T. and W. Knoll. (2003). *J. Electroanal. Chem.* **543**, 51–59.
- [11] Raether, H. (1988). *Excitation of Plasmons and Interband Transitions by Electrons*. Berlin: Springer.
- [12] Tamada, K., T. Ishida, W. Knoll, and H. Fukushima. (2001). *Langmuir* **17**, 1913–1921.
- [13] Stankovic, R. I., S. Jovanovic, L. Ilic, E. Nordmeier, and M. D. Lechner. (1991). *Polymer* **32**, 235–240.
- [14] Knoll, W., G. Schmidt, E. Sackmann, and K. Ibel. (1983). *J. Chem. Phys.* **79**, 3439–3442.